Study of Morphology and Magnesium Purity, Formed by Vapor Phase Through Silicothermic Reduction

AMIR GORJI, MASOUD PANJEPOUR, and MEHDI AHMADIAN

This article describes the influence of temperature profile on the morphology and impurity distributions of magnesium vapor condensation during silicothermic reduction of calcined dolomite. The formation of magnesium crystals was comprehensively analyzed by optical microscopy, scanning electron microscopy (SEM), and inductively coupled plasma (ICP). The results showed that the temperature changed the morphology and purity of condensation products in the condenser. When the temperature of the condenser zone was lower than 250 °C, the magnesium vapor condensation was fine and noncompacted. The crystal growth of magnesium occurred in the range of 250 °C and 380 °C. It was found that crystal magnesium became coarser and denser at higher temperatures. Based on the analysis of crystallized magnesium, the impurity distributions decreased at temperatures higher than those of the condenser. Furthermore, this indicates that the impurity contents with less than 0.04 pct were distributed randomly through the condenser.

https://doi.org/10.1007/s11663-018-1357-x

I. INTRODUCTION

THE use of magnesium in different industries, such as aerospace and automobile manufacturing, is significant due to its distinctive characteristics and properties such as light atomic weight and high strength/density ratio.[1,2] Furthermore, pure magnesium is widely used in the production of strategic and important metals such as uranium and titanium.[3] Commercial magnesium was produced through two main approaches, *i.e.*, electrolysis and thermal methods.[4] The thermal methods consist of two techniques of silicothermic and carbothermic.[5–7] Silicothermic reduction requires less capital cost and is easily produced at small scales.[3,7] Compared to other methods, this method is more suitable for the production of high-purity (about 99.95 pct) magnesium.[3,8–11] The silicothermic reduction method extracts magnesium from dolomite, and as a reductant agent, ferrosilicon is used to reduce MgO in dolomite ores.[12–14] This process, the so-called Pidgeon process, is carried out in a reactor with external heating at a temperature of 1150 °C to 1300 °C.[3,15] This process is represented by Eq. [1]:

$$2CaO(s) + 2MgO(s) + Si(s) \rightarrow 2Mg(g) + Ca_2SiO_4(s) \quad [1]$$

This reaction is endothermic and is carried out in steel retorts. The final step is to condense magnesium vapor in a steel condenser to deposit magnesium crystals.[3,16,17]

Various parameters, such as temperature, impurities, technical parameters, reductant agent, and reducing agent, are effective in the production of magnesium; furthermore, some have significant effects on the deposit of magnesium vapor. The effect of these parameters on the carbothermic process has been extensively studied. Yang *et al.*[18] studied the manner of magnesium formation in the carbothermic reduction of dolomite by using a multilevel condenser. The temperature among the levels was different (923 K, 1023 K, 1123 K, and 1223 K). Their results showed that the temperature gradient was effective for the purity and morphology of magnesium in the condenser. In other research, Yang *et al.*[19] studied the effect of the temperature on the morphology of magnesium nucleation by using the carbothermic process. The results showed that this process was controlled by the temperature and the rate of oxidation reduced when the temperature gradient decreased. Therefore, the quality of magnesium formed in these zones rises significantly at high temperatures. In another study, Yang *et al.*[20] studied the effect of temperature on the deposit of the impurities of alkaline metals, such as sodium and calcium, in different zones of the condenser by using the carbothermic process. This study revealed that the purity of the magnesium formed in a high-temperature zone was

AMIR GORJI, MASOUD PANJEPOUR, and MEHDI AHMADIAN are with the Department of Materials Engineering, Isfahan University of Technology, 84156-83111, Isfahan, Iran. Contact email: a.gorji@ma.iut.ac.ir

Manuscript submitted August 25, 2017.
Article published online July 26, 2018.

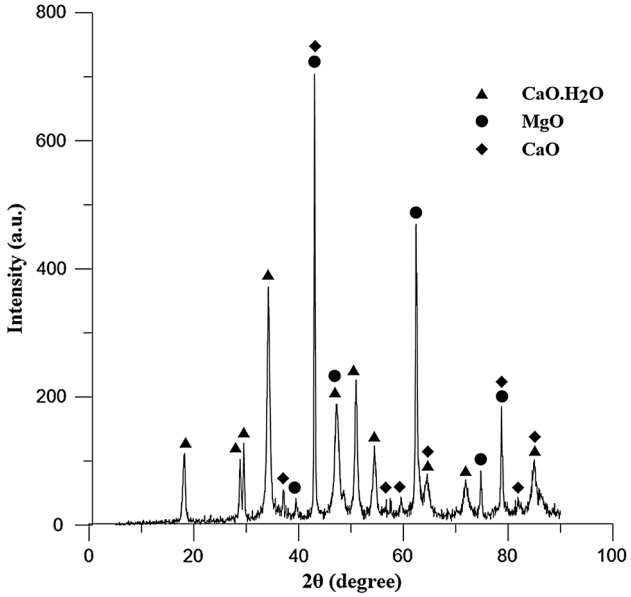

Fig. 1—X-ray pattern of calcined dolomite powder.

Table I. Chemical Composition of Calcined Dolomite Powder (Mass Percent)

Composition	CaO	MgO	Fe_2O_3	SiO_2	Al_2O_3	LOI
Percent Weight	49.14	27.85	0.64	0.12	0.02	21.9

more than that in other zones. In general, although morphological characteristics were investigated in the carbothermic process, limited studies were performed on the various morphologies of silicothermic reduction and distribution of impurities inside the condenser during this process. Investigation of the temperature gradient, morphology, and distribution of impurities is necessary to improve the performance of the silicothermic process. This article focuses on the effect of temperature on the morphological characteristics and distribution of impurities in silicothermic reduction. The morphology of the samples observed by scanning electron microscopy (SEM) and the composition of the magnesium formed were examined by inductively coupled plasma (ICP) and X-ray diffraction (XRD).

II. MATERIALS AND EXPERIMENTAL METHOD

The calcined dolomite powder (1 μm in average diameter), calcium fluoride (0.5 μm in average diameter), and ferrosilicon powder (2 μm in average diameter) were used as the starting raw materials. Figure 1 and Table I show the X-ray diffraction pattern and chemical composition of calcined dolomite, respectively. Dolomite, ferrosilicon, and calcium fluoride powder were mixed with weight percentage according to Table II. The mixture was compacted into briquettes of 60 mm in diameter under 120 MPa.

Table II. Composition of the Charged Briquettes in the Retort

Composition	Dolomite	Ferrosilicon	Calcium Fluorine
Percent Weight	70	26.5	3.5

The reduction tests were carried out by charging the briquettes into a retort furnace at 1200 °C. This retort furnace was made of alloy steel with a condenser, a water-circulating system, and vacuum connections, as shown schematically in Figure 2. Then, the retort valve closed and the vacuum pump started working to reduce the pressure inside the condenser as required (3 Pa). Five thermocouples were used to measure the temperature in different zones (Figure 2(c)), while local temperature measurements along the condenser produced the temperature profile (Figure 3(γ)). After 7 hours, the process was completed. Then, the retort valve was opened and the magnesium crystals formed on the lining of the condenser were discharged. The samples were collected from different parts of the magnesium batch and cross-sectional samples were prepared by acid cleaning. The samples were dipped in 5 pct nitric acid solution for 3 minutes followed by washing with water and drying by air blowing. Ultimately, the product was examined by optical microscopy (model BH2-UMA manufactured by Olympus Company); SEM (model XL30SERIES manufactured by Philips Company); and ICP (model Optima8000 manufactured by Perkin Elmer Company) to analyze the structure and manner of distribution of impurities.

III. RESULTS AND DISCUSSION

A. *Magnesium Morphology at the Length of Condenser*

Figure 3 shows the optical micrographs of the morphology of the magnesium product inside the condenser. It is observed that the morphology of the magnesium crystals is different in the zones of the condenser, so the condenser can be divided into three zones: I, II, and II.

This process can be attributed to the formation of supersaturated magnesium vapor with a decreasing temperature in the condenser. The temperature is an important factor influencing the nucleation and growth of magnesium atoms during the vapor → solid transition. This leads to the formation of the magnesium nuclei on the surface of the condenser. The nucleation radius of nuclei is calculated by Eq. [2][21]:

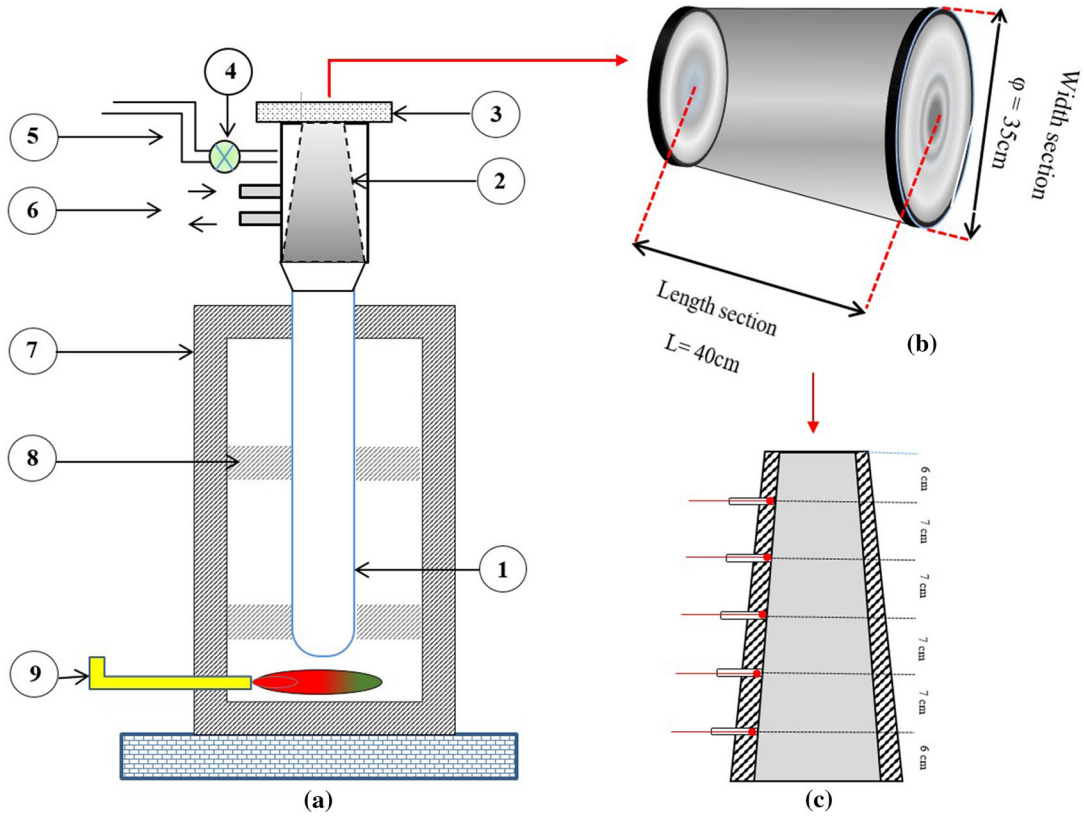

Fig. 2—(*a*) Schematic of the experimental apparatus: (1) retort, (2) condenser, (3) retort valve, (4) vacuum valve, (5) vacuum joint, (6) water-circulating system, (7) furnace body, (8) retort keeper, and (9) flame torch; (*b*) dimension of condenser mentioned in part (a2); and (*c*) location of thermocouples in condenser.

$$r^* = \left(\frac{2\sigma\upsilon T_{eq}}{\Delta H_{sub}}\right)\frac{1}{\Delta T} \qquad [2]$$

where σ is the surface energy, υ refers to the atomic volume of the nucleus, ΔH_{sub} stands for the enthalpy of sublimation, T_{eq} represents equilibrium temperature, and ΔT is the value of undercooling.

It is concluded that the driving force of nucleation (ΔT) increases the rate of nucleation at lower temperatures and the rate of growth increases at higher temperatures. Under these conditions, magnesium formation is controlled by diffusion parameters and its morphology is controlled by growth mechanisms. Thus, the nuclei formed in zone I did not grow (temperature range was between 150 °C and 250 °C). The image obtained from this zone (Figure 3(a)) clearly confirms this fact. It can be seen that the uniform and noncondensed structure would result in the generation of numerous nuclei, preventing their growth. Figure 4 shows the microstructure of the magnesium product in zone I. Three-dimensional nucleation controlled by the island growth mechanism was observed.

According to Figures 3(b) and (c), the magnesium vapor has a dense crystal structure compared to that in Figure 3(a). Figure 5 illustrates SEM micrographs of magnesium crystals collected at the second condenser zone (II) (temperature range was between 250 °C and 350 °C). The cross section of this zone is shown in Figure 6. The magnesium formed in zone II has a dense hexagonal crystal structure with a layer growth mechanism (Figure 6). It can be seen that the main planes have the lowest surface energy and the edges have the highest energy. Therefore, these planes have grown initially by two-dimensional (2-D) growth that is in accordance with equal and coaxial [0001] faces.

In contrast, Cho and Fawcett[22] focused on the growth morphology of Mg-chlorite ($5MgO{\cdot}Al_2O_3{\cdot}3SiO_2{\cdot}4H_2O$) with a hexagonal structure originating from the vapor phase. According to their results, the lateral growth rate was lower than that of the nucleation frequency on the main planes. If it indeed occurred, this plays an important role in the growth of magnesium in zone II. It can be found that as the thickness of each plane increases, the next plane grows

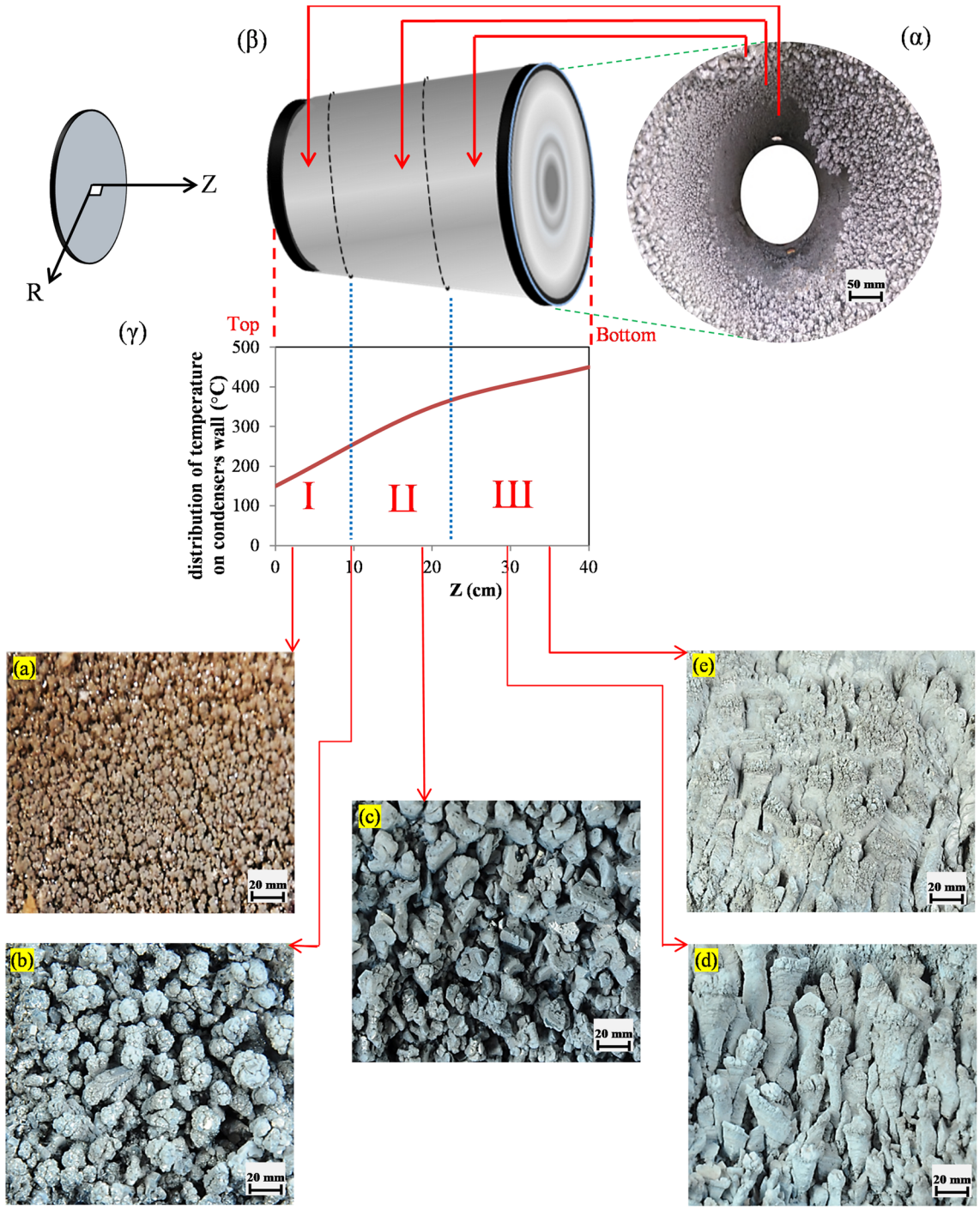

Fig. 3—Details of the condenser and the morphology of magnesium formed in different zones: (α) front view of a batch of magnesium formed inside the condenser; (β) schematic representation of different zones of the condenser; and (γ) temperature profile along the condenser: (*a*) magnesium formed in zone I, (*b*) magnesium formed between zones I and II, (*c*) magnesium formed in zone II, (*d*) magnesium formed in zone III, and (*e*) magnesium formed in the end of zone III.

on its high-energy regions, including crystalline defects and edges. Therefore, the magnesium of crystals with polygonal shapes was mainly observed in zone II.

According to Figures 3(d) and (e), the massive magnesium crystals with compact morphology were collected at the third condenser zone (III) (temperature range was between 350 °C and 450 °C). It is concluded that the high temperature decreased the rate of nucleation and increased the rate of growth in this zone. Figure 7 provides SEM micrographs of magnesium crystals collected at zone III.

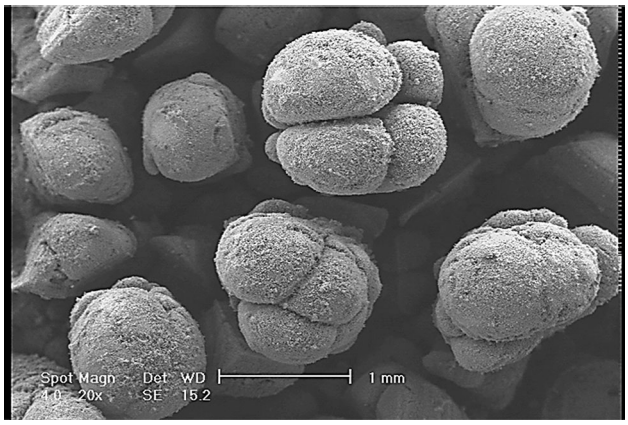

Fig. 4—SEM photomicrograph of the magnesium formed in zone I.

Under these conditions, the growth rate was controlled by three-dimensional nucleation and the spiral growth mechanism, resulting in the appearance of cauliflower-like morphologies. According to the results obtained by Sunagawa,[23] the mechanism of the layer growth was limited by the activation energy of 2-D nucleation. Growth could not begin unless the activation energy required for 2-D nucleation was overcome. However, the mechanism of spiral growth is not required to provide the activation energy at high temperatures. The spiral growth starts with polygonal nucleation, which eventually shows morphological progress by making smooth crystals at their surfaces over which impact structures are created. The result of the growth mechanism shows that the spiral growth mechanism takes place with temperature after the layer growth mechanism. At the end of zone III, the temperature is high and the crystals are allowed to settle rapidly on the edges of the condenser (Figure 3(d)). These factors determine the morphologies of crystals including number of nuclei, energy barrier, and temperature. As a result, the cauliflower-like branch morphology will appear (Figure 8).

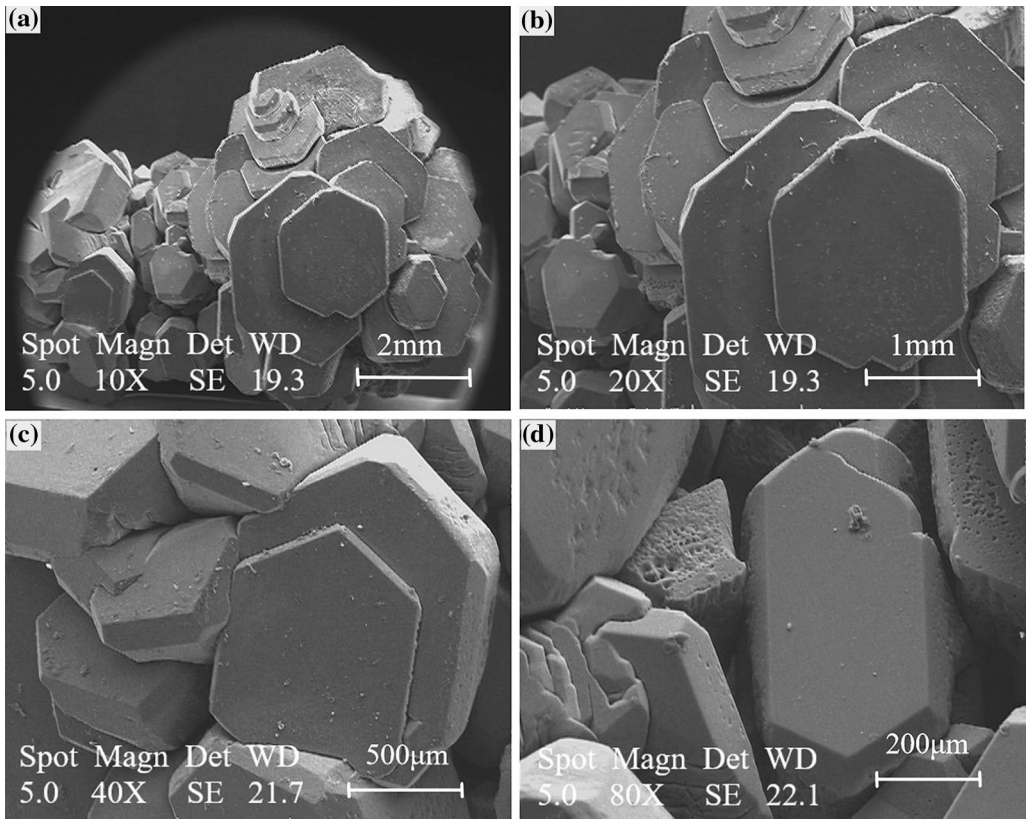

Fig. 5—SEM of zone II in different magnifications: (*a*) 10 times, (*b*) 20 times, (*c*) 40 times, and (*d*) 80 times.

B. *Magnesium Morphology at the Cross Section of the Condenser*

The cross section of the condenser was investigated in detail for nucleation and the growth mechanism. The magnesium vapor condenses in the crystalline structure on the water circulator of the condenser (Figure 3 (direction of *R*-axis)). This creates a thermal gradient due to the continuous heat transfer from the wall of the condenser. As shown in Figure 9, at the initial stage of deposition and when clusters achieve a critical size in the condenser, precipitation of initial particles on the wall of the condenser takes place. In fact, these fine particles were observed on the entire surface of the condenser (zones I–III).

As the thickness of the magnesium formed increases, the rate of heat transfer decreases. This results in larger crystalline grains for particles than those in the previous layer. In addition, the temperature gradient generated at the cross section of the condenser provides directional growth, bringing about the columnar structures in the condenser, as shown in Figure 10.

C. *Distribution of Impurities at the Length of the Condenser*

There are some oxide impurities in dolomite, which are reduced to elements, such as Zn, Ca, K, Na, Si, and Fe, and enter into magnesium produced during the condensation of vapor in silicothermic process (Table III). In this process, the concentration of impurities and their distribution in the final product depend on the composition of raw materials and the temperature profile in the condenser, respectively. Figure 11 shows the influence of temperature on the concentration of impurities in different zones of the condenser. As shown in this figure, the temperature profile along the condenser brings about a change in magnesium purity in the different zones (I–III), except the impurity elements such as K, Si, and Fe with less than 0.04 pct (*i.e.*, this concentration of elements was distributed randomly through the condenser). In fact, with increasing temperature, the concentration of impurities in condensation products, such as Zn, Ca, and Na, is decreased.

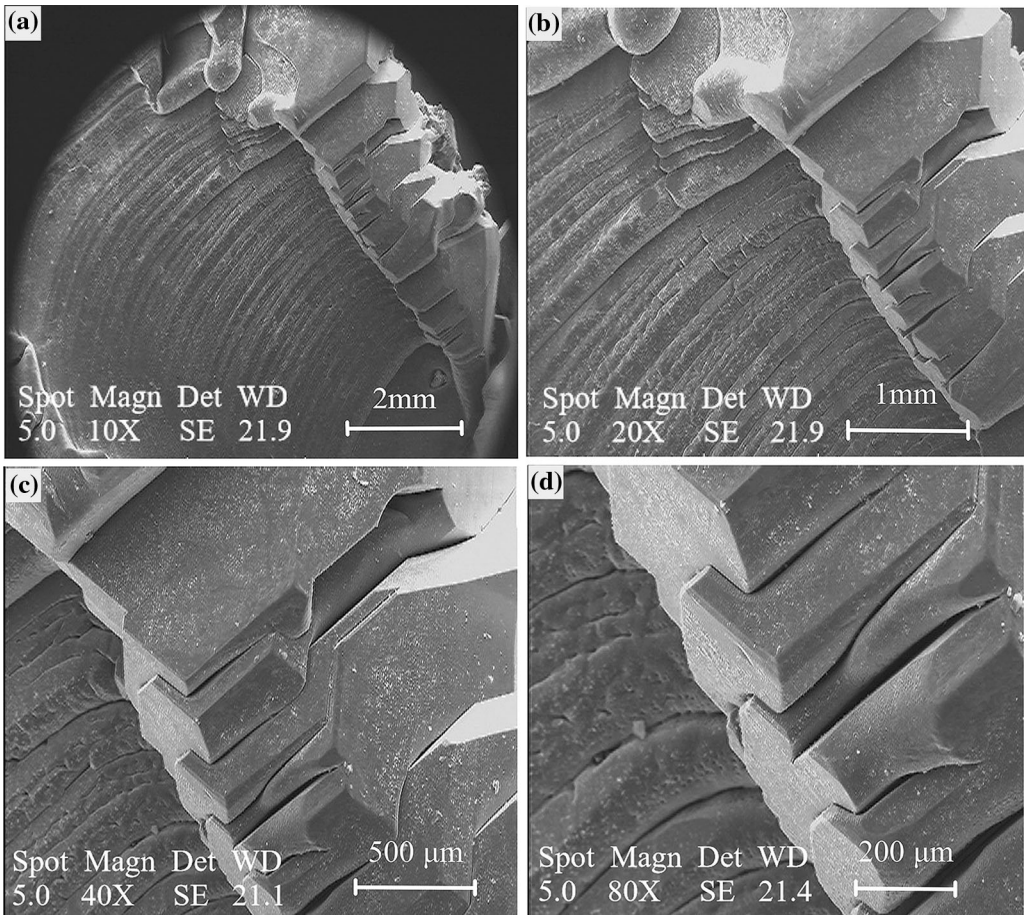

Fig. 6—SEM of the cross-sectional zone II condenser in different magnifications: (*a*) 10 times, (*b*) 20 times, (*c*) 40 times, and (*d*) 80 times.

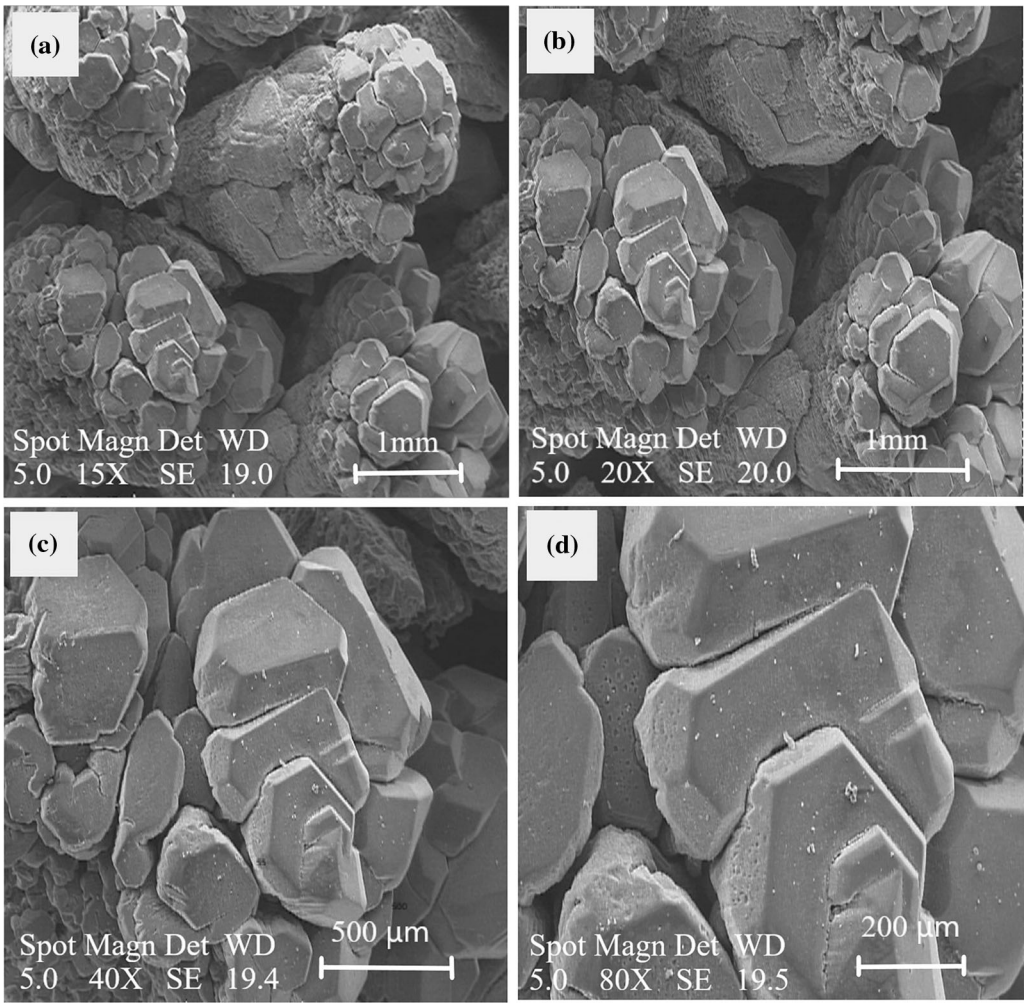

Fig. 7—SEM of zone III in different magnifications: (*a*) 10 times, (*b*) 20 times, (*c*) 40 times, and (*d*) 80 times.

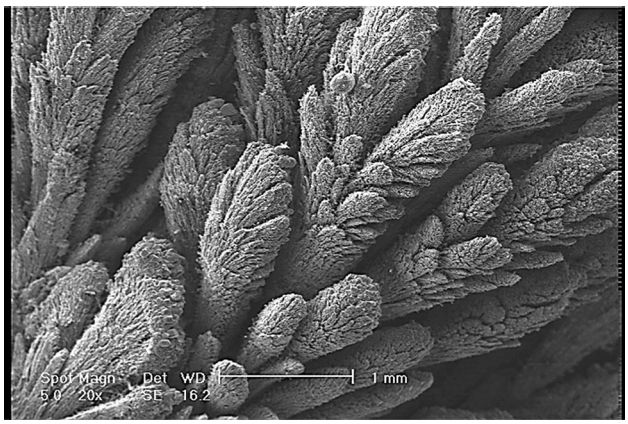

Fig. 8—SEM photomicrograph of crystals at the end of zone III.

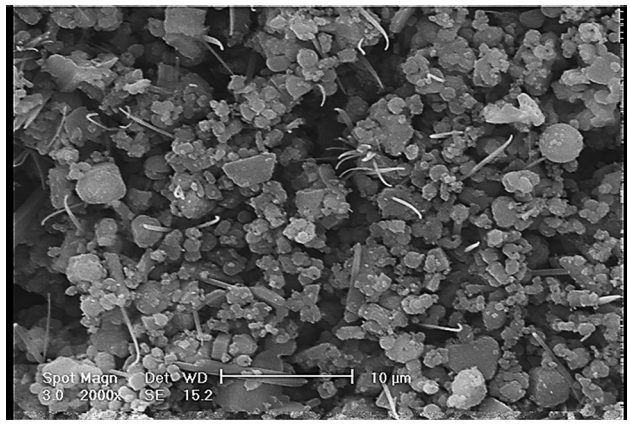

Fig. 9—SEM photomicrograph of initial particles on the wall of the condenser.

Fig. 10—Directional growth of the crystals at the cross section of the condenser.

Table III. Chemical Composition of Magnesium Formed in Different Zones of the Condenser (RSD Percent < 2)

Composition	Zone I (Wt Pct)	Zone II (Wt Pct)	Zone III (Wt Pct)
Mg	99.593	99.791	99.865
Zn	0.170	0.077	0.063
Ca	0.110	0.100	0.004
K	0.030	0.011	0.030
Na	0.090	0.012	0.020
Si	0.020	0.003	0.005
Fe	0.007	0.006	0.018

RSD: range and standard deviation.

Therefore, the concentration of magnesium purity from zone III (350 °C to 450 °C) is more than that of other zones.

IV. CONCLUSIONS

This study investigated the morphology and purity content of magnesium through the silicothermic reduction process. The results obtained are as follows.

1. The length of condenser as a function of temperature in the range of 150 °C to 450 °C is shown. Therefore, the condenser can be divided into three zones: cool, medium, and warm. In the cool zone, the magnesium vapor directly turns into solid. Therefore, it will have a uniform, noncondensing, and powdery structure. By moving toward the hot regions, the structure of magnesium crystals will be more compressed and coarser.
2. The cross section of the condenser creates a thermal gradient due to heat transfer from the wall of the condenser. Therefore, it provides directional growth, bringing about the columnar structures in the condenser.
3. The experimental results show that the temperature profile changed the distribution of impurities in the final product along the condenser. The concentration of impurities decreased with an increase in temperature, except the impurity elements with less than 0.04 pct. These elements were distributed randomly through the condenser.

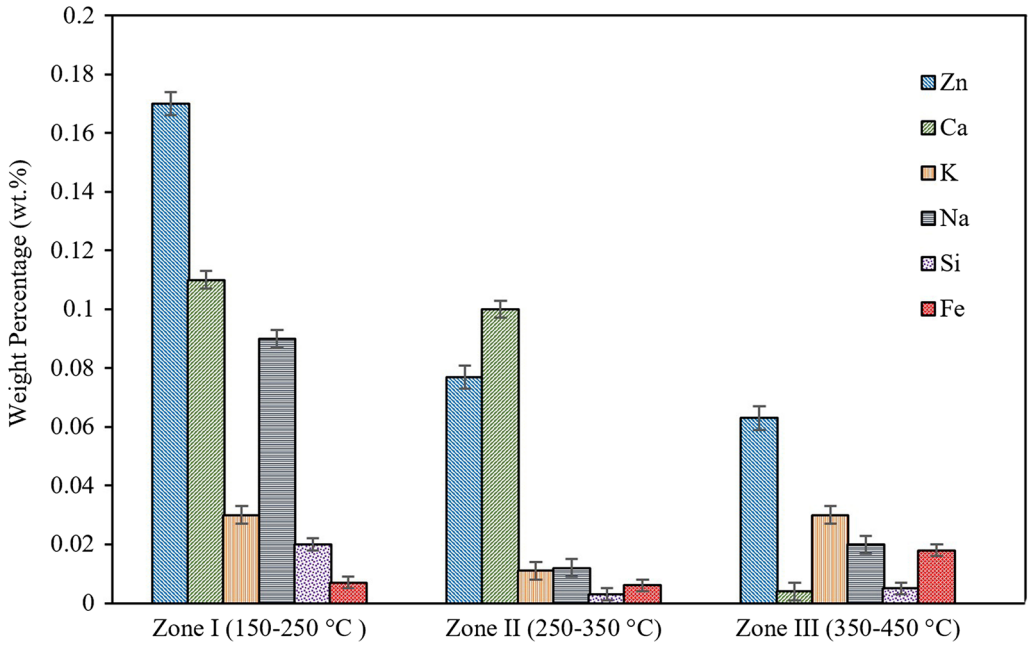

Fig. 11—Comparison of impurities in different zones of the condenser.

REFERENCES

1. Y. Tian, T. Qu, B. Yang, Y.N. Dai, B.Q. Xu, and S. Geng: *Metall. Mater. Trans. B*, 2012, vol. 43B, pp. 657–61.
2. X.J. Wang, D.K. Xu, R.Z. Wu, X.B. Chen, Q.M. Peng, L. Jin, Y.C. Xin, Z.Q. Zhang, Y. Liu, X.H. Chen, G. Chen, K.K. Deng, and H.Y. Wang: *J. Mater. Sci. Technol.*, 2017, in press.
3. F. Habashi: *Handbook of Extractive Metallurgy*, Wiley, New York, NY, 1997, pp. 1160–62.
4. L. Rongti, P. Wei, and M. Sano: *Metall. Mater. Trans. B*, 2003, vol. 34B, pp. 433–37.
5. Y. Tian, B.Q. Xu, C.B. Yang, B. Yang, T. Qu, H.X. Liu, Y.N. Dai, and D.C. Liu: *Metall. Mater. Trans. B*, 2014, vol. 45B, pp. 1936–41.
6. A. Krishnan, X.G. Lu, and U.B. Pal: *Metall. Mater. Trans. B*, 2005, vol. 36B, pp. 463–73.
7. K.N. Solanki, D. Orlov, A. Singh, and N.R. Neelameggham: *Magnesium Technology 2017,* Springer, Switzerland, 2017, pp. 107–11, 199–202, and 107–11.
8. R.B. Li, S.J. Zhang, L.J. Guo, and J.J. Wei: *Int. J. Heat Mass Transf.*, 2013, vol. 59, pp. 328–37.
9. D. Fu, Y. Wang, J. Peng, Y. Di, S. Tao, and N. Feng: *Adv. Chem. Eng. II*, 2012, vols. 550–553, pp. 1779–83.
10. W. Wulandari, A. Rhamdhani, G. Brooks, and B.J. Monaghan: *Eur. Metall. Conf. on GDMB Society for Mining,* EMC, Austria, 2009, pp. 1401–15.
11. I.M. Morsi and H.H. Ali: *Int. J. Miner. Process.*, 2014, vol. 127, pp. 37–43.
12. D.X. Fu, T.A. Zhang, L.K. Guan, Z.H. Dou, and M. Wen: *JOM*, 2016, vol. 68, pp. 3208–13.
13. B. Mehrabi, M. Abdellatif, and F. Masoudi: *Int. J. Mater. Sci. Eng.*, 2011, vol. 8, pp. 18–24.
14. C. Wang, C. Zhang, S.J. Zhang, and L.J. Guo: *Int. J. Miner. Process.*, 2015, vol. 142, pp. 147–53.
15. Y. Aviezer, L. Birnhack, A. Leon, E. Aghion, and O. Lahav: *Hydrometallurgy*, 2017, vol. 169, pp. 520–33.
16. M. Bugdayci, A. Turan, M. Alkan, and O. Yucel: *High Temp. Mater. Proc.*, 2018, vol. 37, pp. 1–8.
17. H. Halmann, A. Frei, and A. Steinfeld: *Ind. Eng. Chem. Res.*, 2008, vol. 47, pp. 2146–54.
18. C.B. Yang, Y. Tian, T. Qu, B. Yang, B.Q. Xu, and Y.N. Dai: *J. Magn. Alloys*, 2014, vol. 2, pp. 50–58.
19. C.B. Yang, Y. Tian, T. Qu, B. Yang, B.Q. Xu, and Y.N. Dai: *Trans. Nonferr. Met. Soc. China*, 2014, vol. 24, pp. 561–69.
20. C.B. Yang, Y. Tian, T. Qu, B. Yang, B.Q. Xu, and Y.N. Dai: *J. Magn. Alloys*, 2013, vol. 1, pp. 323–29.
21. A.K. Mahapatra, J. Wang, H. Zhang, and M. Han: *Lett. J. Explor. Front. Phys.*, 2016, vol. 115, pp. 1–6.
22. M. Cho and J.J. Fawcett: *Am. Miner.*, 1986, vol. 71, pp. 78–84.
23. I. Sunagawa: *Crystals Growth, Morphology and Perfection*, 1st ed., Cambridge University Press, New York, NY, 2005, pp. 45–47.